MAPP Name	Number Changed	Number Measured	Percent Changed	Z Score	PermuteP	AdjustedP
Mm_Striated_muscle_contraction	5	17	29.4	4.61	0	0.099
Mm_Nuclear_Receptors	4	20	20.0	3.08	0.02	0.59
Mm_Steroid_Biosynthesis	2	8	25.0	2.58	0.04	0.81
Mm_Gluthation_Metabolism_KEGG	3	10	30.0	3.15	0.02	0.60
Mm_B_Cell_Receptor_NetPath_12	8	60	13.3	2.36	0.03	0.91
Mm_Id_NetPath_5	3	18	16.7	2.26	0.05	0.94

Supplemental Table S1. MAPPFinder results showing the most up- and down-regulated pathways.

A fold change of 1.5 and a *p*-value of <0.05 were used as the criteria for gene expression changes in the *Rp58* KO mouse cortex compared with WT.

Number changed, number of genes changed; Number measured, number of genes measured on the chip; Number on MAPP, number of genes on the MAPP; Percent changed, number changed divided by the number measured. The *z*-score assumes a hypergeometric distribution. Permute P, *p*-value calculated from repeated random sampling trials; Adjusted *p*-value, *p*-value derived from statistically multiplexed tests.

Supplemental Table S2. List of up- and down-regulated genes identified in Table S1.

MAPP Name	Symbol	*Rp58* KO_Intensity	WT_Intensity	Ratio(KO/WT)	Log2Ratio(KO/WT)	Description	Accession Number
Mm_Striated_muscle_contraction	Mybpc3	103.1447368	46.57910043	2.214399503	1.146915524	Mus musculus myosin binding protein C, cardiac (Mybpc3), mRNA.	NM_008653
	2300003C06Pik	113.5	58.96943773	1.92472583	0.944652954	Mus musculus adult male tongue cDNA, RIKEN full-length enriched library, clone: 2310032K21.	AK009578
	Myl1	98.80263158	61.4738676	1.607229794	0.684576214	Mus musculus 18 days embryo cDNA, RIKEN full-length enriched library, clone:1100001J17.	AK003182
	Myom1	96.81578947	64.4066868	1.503194688	0.588031874	Mus musculus myomesin 1 (Myom1), mRNA.	NM_010867
	Tnnc2	107.9736842	74.55621842	1.448218358	0.534279144	Mus musculus troponin C, fast skeletal (Tncs), mRNA.	NM_009394
Mm_Nuclear_Receptors	Hnf4a	70.39473684	39.67544176	1.774264727	0.827221281	Mus musculus hepatic nuclear factor 4 (Hnf4), mRNA.	NM_008261
	Nr1h2	82.09210526	55.24574593	1.485944372	0.571380108	602093563F1 NCI_CGAP_Co24 Mus musculus cDNA clone IMAGE:4208055 5, mRNA sequence.	BF579673
	Nr4a1	100.3815789	68.70705653	1.461008287	0.546964361	Mus musculus nuclear receptor subfamily 4, group A, member 1 (Nr4a1), mRNA.	NM_010444
	Nrld2	367.3026316	258.5411937	1.420673535	0.506575067	Mus musculus orphan nuclear receptor RVR mRNA, complete cds.	U12142
Mm_Steroid_Biosynthesis	Hsd3b2	360.1973684	196.5647924	1.832461266	0.873782704	Mouse 3-beta-hydroxysteroid dehydrogenase/delta-5-delta-4 isomerase mRNA sequence.	M75886
	F13b	49.94736842	32.88711866	1.518751732	0.602886054	Mus musculus coagulation factor XIII, beta subunit (F13b), mRNA.	NM_031164
Mm_Gluthation_Metabolism_KEGG	Hcls1	29.65131579	121.8685236	0.243305777	-2.039157522	Mus musculus hematopoietic cell specific Lyn substrate 1 (Hcls1), mRNA.	NM_008225
	Cd79a	57.22368421	90.02766352	0.63562334	-0.653755993	Mus musculus immunoglobulin-associated alpha (Iga), mRNA.	NM_007655
	Fyn	83.46052632	118.729748	0.702945367	-0.508515528	Mus musculus Fyn proto-oncogene (Fyn), mRNA.	NM_008054
Mm_B_Cell_Receptor_NetPath_12	Idh1	2421.552632	5103.731515	0.474467088	-1.075620077	Mus musculus isocitrate dehydrogenase 1 (NADP+), soluble (Idh1), mRNA.	NM_010497
	Dusp6	207.3157895	430.2676437	0.481829839	-1.053404355	Mus musculus RIKEN cDNA 1300019I03 gene (1300019I03Rik), mRNA.	NM_026268
	Mapk8	150.4868421	280.9739652	0.535589986	-0.900799108	Mus musculus mitogen activated protein kinase 8 (Mapk8), mRNA.	NM_016700
	Actr3	1074.965003	1867.871544	0.575502639	-0.797105551	Mus musculus actin-related protein 3 (Arp3) mRNA, partial cds.	AF307855
	Casp9	91.51973684	154.5249711	0.592265031	-0.755685187	Mus musculus caspase 9 (Casp9), mRNA.	NM_015733
	Gsta2	148.8684211	240.7712751	0.618298096	-0.693625531	Mus musculus glutathione S-transferase, alpha 2 (Yc2) (Gsta2), mRNA.	NM_008182
	Gstm3	201.2631579	306.0841701	0.657541871	-0.604845329	Mouse, glutathione transferase GT9.3 mRNA, 3' end.	J03953
	Arpc1b	176.9736842	268.8637286	0.658228185	-0.603340291	Mus musculus actin-related protein complex 1b (Arpc1b) mRNA, complete cds.	AF162768
Mm_Id_NetPath_5	Id3	2376.010569	913.5215903	2.60093532	1.379030523	Mus musculus inhibitor of DNA binding 3 (Idb3), mRNA.	NM_008321
	MSC	156.7697368	70.23113392	2.232197148	1.158464452	Mus musculus musculin (Msc), mRNA.	NM_010827
	Id1	580.3026316	328.9535692	1.764086746	0.818921505	Mus musculus transcription factor Id1B (Id1B) mRNA, complete cds.	U43884

Supplementary Table S3. Comparison of *Ids*- and *Id*-related gene expression profiles in the cortices of *Rp58* KO and control mice.

.

Family Name	Symbol	*Rp58* KO_Intensity	WT_Intensity	Ratio(KO/WT)	Log2Ratio(KO/WT)	Description	Accession Number
Id	*Id1*	580.3026316	328.9535692	1.764086746	0.818921505	Mus musculus transcription factor Id1B (Id1B) mRNA, complete cds.	U43884
	Id2	3606.508275	3491.986166	1.032795694	0.04655489	Mus musculus inhibitor of DNA binding 2 (Idb2), mRNA.	NM_010496
	Id3	2376.010569	913.5215903	2.60093532	1.379030523	Mus musculus inhibitor of DNA binding 3 (Idb3), mRNA.	NM_008321
	Id4	328.75	227.8207364	1.443020531	0.529091827	Mus musculus inhibitor of DNA binding 4 (Idb4), mRNA.	NM_031166
Cip/Kip	*p21*	132.25	92.82867062	1.424667607	0.510625359	Mus musculus cyclin-dependent kinase inhibitor 1A (P21) (Cdkn1a), mRNA.	NM_007669
	p27	137.8947368	113.6385057	1.21345081	0.279115627	Mus musculus cyclin-dependent kinase inhibitor 1B (P27) (Cdkn1b), mRNA.	NM_009875
	p57	1444.163456	2386.377196	0.605169819	-0.724588055	Mus musculus cyclin-dependent kinase inhibitor 1C (P57) (Cdkn1c), mRNA.	NM_009876
INK4	*p15*	97.09210526	120.7069295	0.804362315	-0.314082603	Mus musculus cyclin-dependent kinase inhibitor 2B (p15, inhibits CDK4) (Cdkn2b), mRNA.	NM_007670
	p16	210.0789474	252.8320821	0.830903047	-0.267247948	Mus musculus strain BALB/cAnPt cyclin dependent kinase inhibitor p16INK4a (Cdkn2a) mRNA.	AF044335
	p18	1165.798749	1074.030642	1.085442727	0.118283605	Mus musculus cyclin-dependent kinase inhibitor 2C (p18, inhibits CDK4) (Cdkn2c), mRNA.	NM_007671
	p19	893.8401639	1008.563786	0.886250504	-0.174213551	Mus musculus cyclin-dependent kinase inhibitor 2D (p19, inhibits CDK4) (Cdkn2d), mRNA.	NM_009878

*

Supplementary Figure S1.

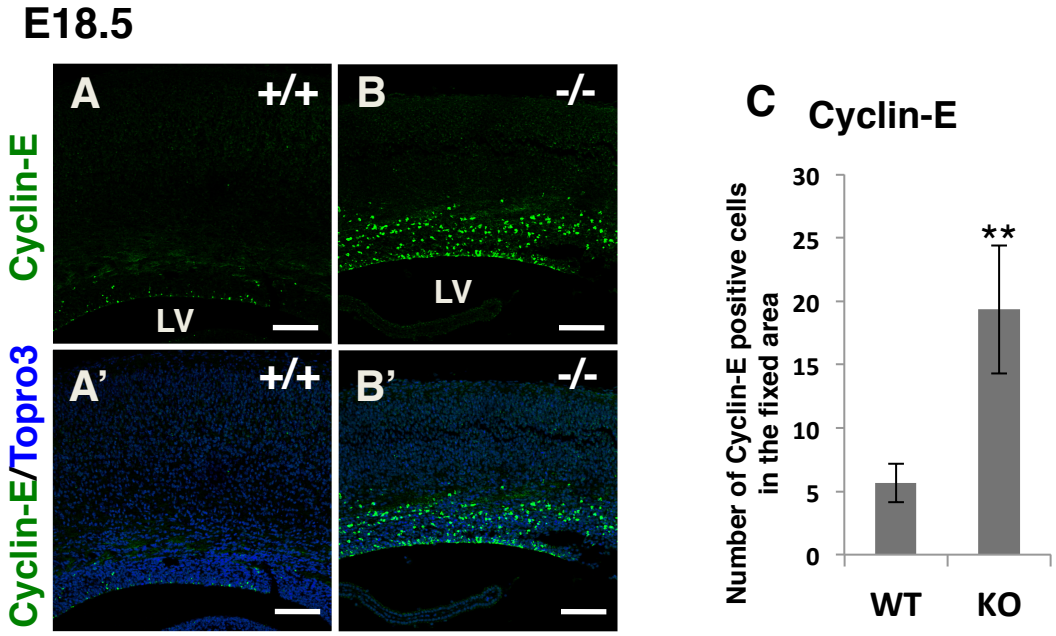

Figure S1. *Rp58* KO cortex showing cell cycle re-entry, even during late gestation. (**A-B'**) Coronal sections of WT and mutant cortex were stained with anti-cyclin-E (green) and Topro3 (blue, nuclear stain). Scale bars: 100 μm. LV: lateral ventricle. (**C**) The number of cyclin-E positive cells in the fixed area was measured (*n*=3).

Supplementary Figure S2.

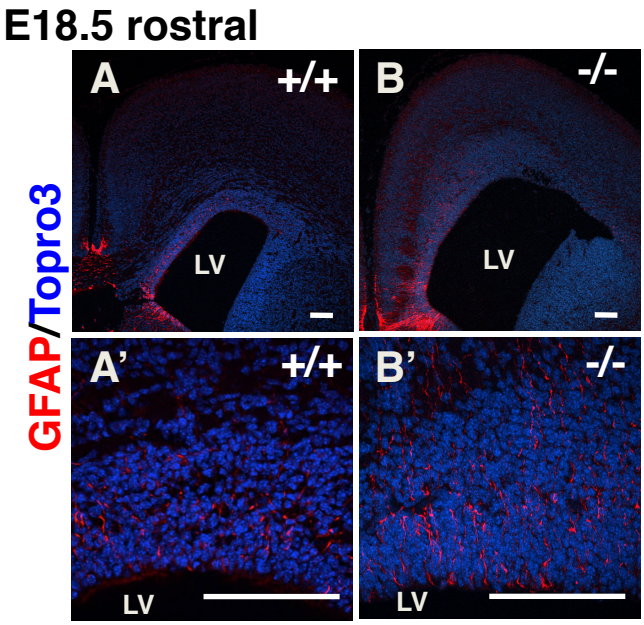

Figure S2. The number of GFAP-positive astrocytes was not clearly increased in the *Rp58* KO rostral cortex compared with the control cortex.
(**A-B'**) Representative images showing staining of coronal sections from WT and mutant mice for GFAP. (**A'**) and (**B'**) represent magnified images from (**A**) and (**B**) , respectively. Nuclei were stained with Topro3. Scale bars: 0.1 mm. LV: lateral ventricle (*n*=3).

Supplementary Figure S3.

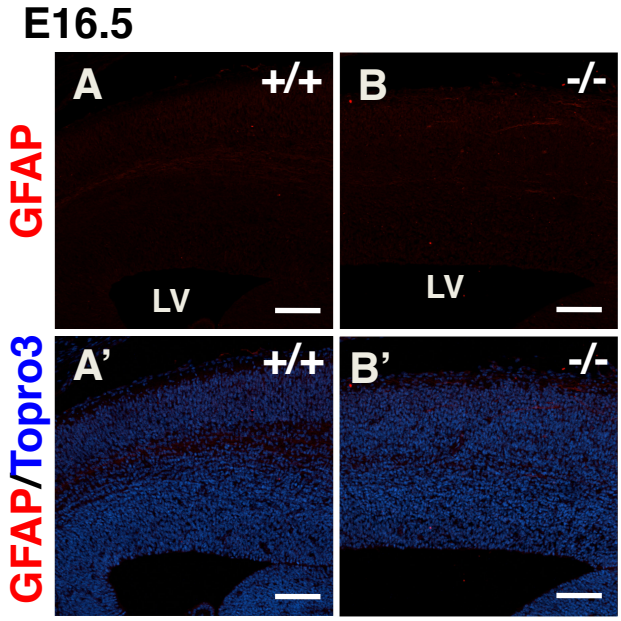

Figure S3. **Astrocytes were not yet present in the E16.5 RP58 mutant or control cortex.** (**A-B'**) Representative immunohistochemical staining of coronal sections for GFAP. Nuclei were stained with Topro3. (**A**') and (**B**') are merged image of GFAP and Topro3. Scale bars: 0.1 mm. LV: lateral ventricle. (*n*=3).

Supplementary Figure S4.

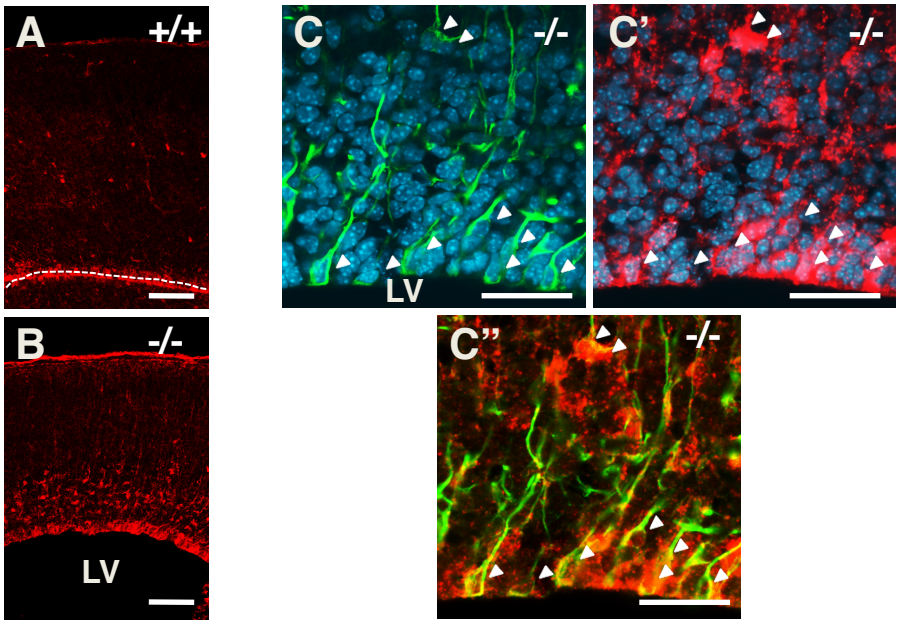

Figure S4. *Rp58* KO mice show incremental increases in S100β-positive astrocytes. (**A,B**) Representative images showing staining for S100β in caudal sections from E18.5 WT (**A**) and mutant mice (**B**). The number of S100β-positive astrocytes was increased in Rp58 KO mice. (**C-C"**) Double immunostaining for S100β and GFAP in the mutant mice. (**C**) shows merged images of GFAP and nuclear staining (DAPI). C' shows merged images of S100β and nuclear staining (DAPI). C" shows merged images of S100β and GFAP. Double-positive cells are indicated by arrowheads. Scale bars: 100 μm (**A,B**), 50 μm (**C-C"**). LV: lateral ventricle. The dotted line in (**A**) indicates the edge of the VZ (*n*=3).

Supplementary Figure S5.

Red font; E-box, ( ); cloning region
Mouse; Ms, Human;Hu

Id1 **(+1189 ~ +1400)**
Ms; cacagctggt----cacatctggg
Hu; cacagctggt----tacatctgga

Id2 **(–2576 ~ –2966)**
Ms; cacatctgg----ctcacagctgtg
Hu; cacatctgg----ctcacagctgtg

Id3 **(–3318 ~ –3028)**
Ms; cacagctgtggg----cccacagctggg
Hu; cacagctgtggg----cccacagctggg

Id4 **(+23271 ~ +23551)**
Ms; cacagctgta----cacagctgtg
Hu; cacagctgta----cacagctgtg

Figure S5. Location and putative RP58-binding sequence in each *Id* genomic region (conserved between mouse and human).
Red font indicates E-box sequences (CANNTG).

Supplementary Figure S6.

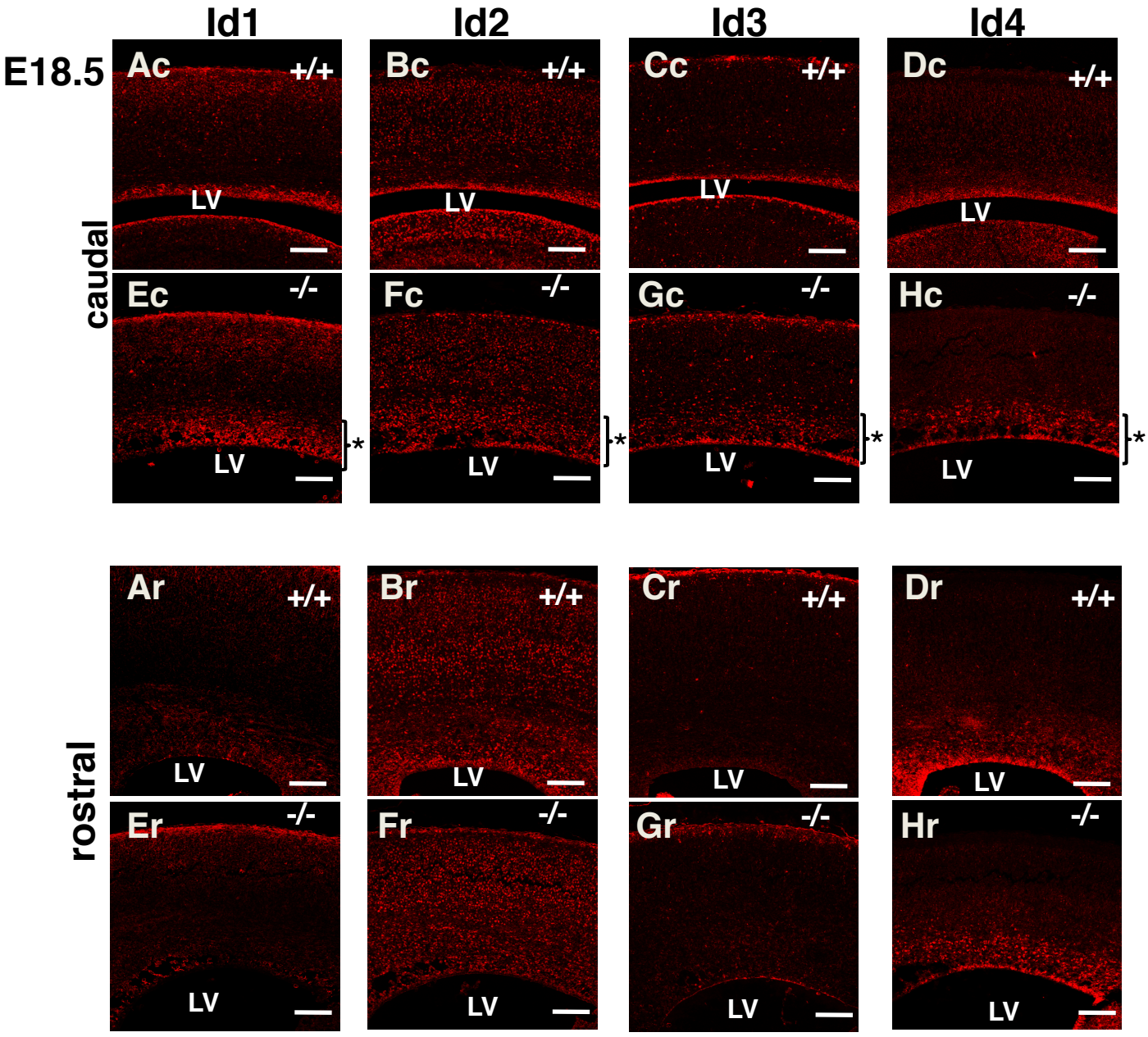

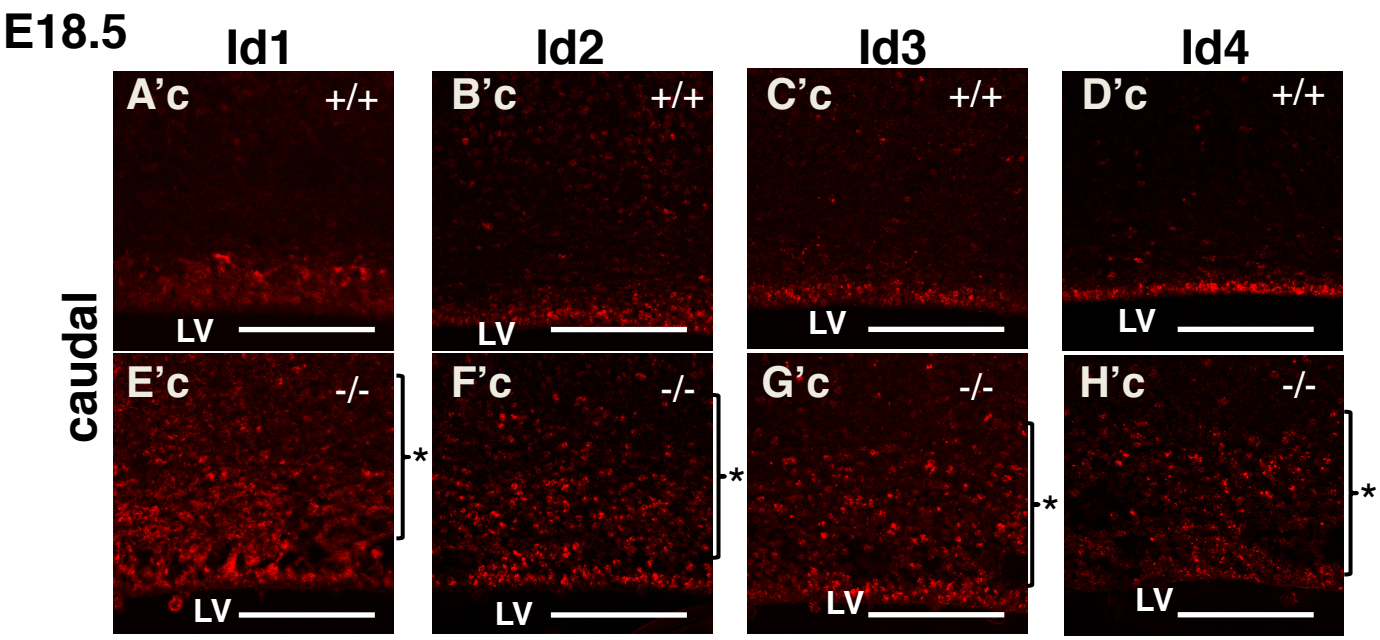

Figure S6. *Rp58* KO mice show ectopic expression of Id proteins in the cerebral cortex. (**Ac-H'c, Ar-Hr)** Representative images showing Id1, Id2, Id3, and Id4 in caudal sections (**Ac-H'c**) and rostral sections (**Ar-Hr**) from E18.5 WT and mutant mice. (**A'c-H'c**) represent magnifications of (**Ac-Hc**), respectively. The stars indicate the regions in which all Id proteins were ectopically expressed in the mutant cerebral cortex around the VZ/SVZ (**Ec-Hc, E'c-H'c**) (star). Scale bars: 100 µm. LV: lateral ventricle (*n*=3).

Supplementary Figure S7.

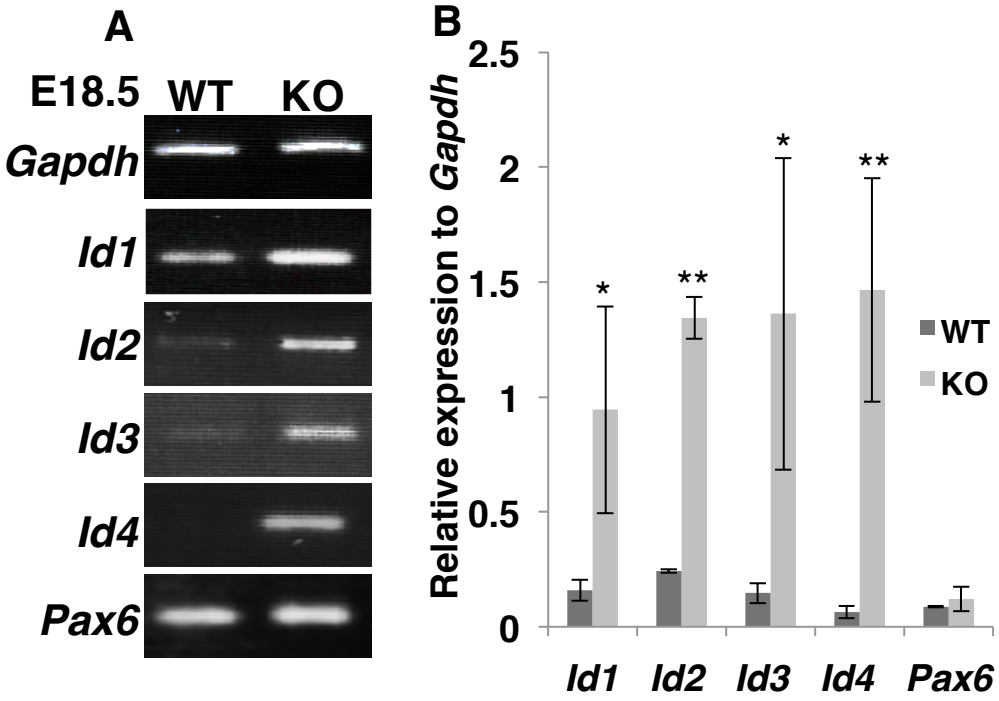

Figure S7. **Expression of *Id1-Id4* mRNAs was upregulated at each neurosphere level in *Rp58* KO mice.**
(**A**) Reverse transcription (RT)-PCR shows the expression levels of endogenous *Id* and *Gapdh* (internal control) mRNAs. (**B**) Semi-quantification of the presented agarose gel image (**A**) was performed using Fiji software. *Pax6* mRNA was used as a negative control. *t*-test: (*) $P < 0.05$, (**) $P < 0.01$. Error bars represent mean ± SD, $n = 5$.

Supplementary Figure S8.

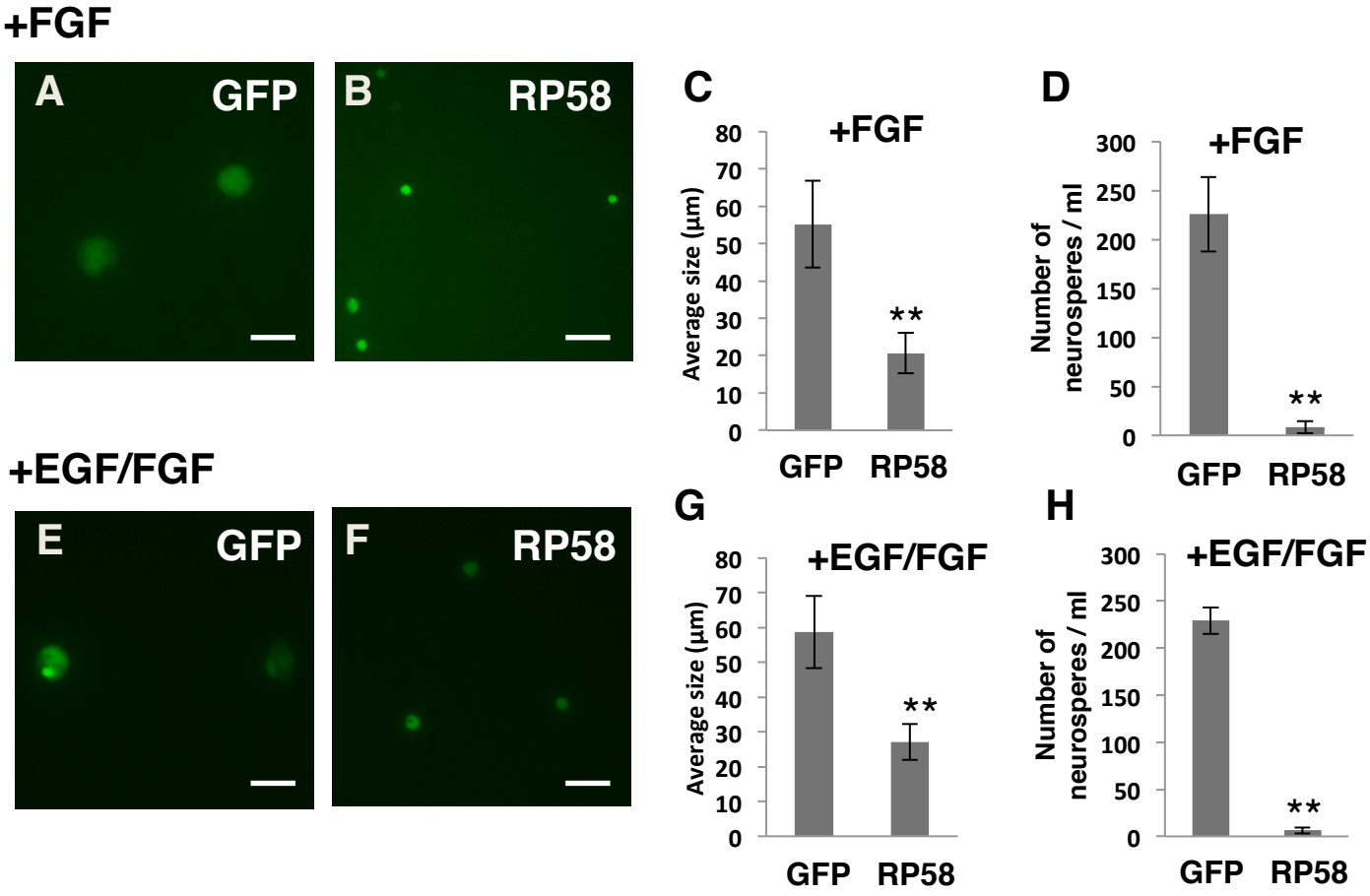

Figure S8. RP58 reduces the self-renewal capacity of neurospheres under FGF2- or EGF- and FGF2-supplemented conditions.
(**A, B, E, F**) Representative images of GFP- expressing neurospheres isolated from the E14.5 cortex and cultured for 7 days in the presence of FGF2 (**A, B**) or EGF and FGF2 (**E, F**). (**C, G**) The average diameter under the conditions in (**A**, **B**) or (**E**, **F**). (**D, H**) The number of neurospheres was counted after replating primary neurosphere cells of (**A**, **B**) or (**E**, **F**) at 0.5×10^5 cells/ml. (**C, D, G, H**) Three independent experiments were performed. (**$P < 0.01$; *t*-test). Error bars indicate the SD. Scale bars: 100 μm.

Supplementary Figure S9.

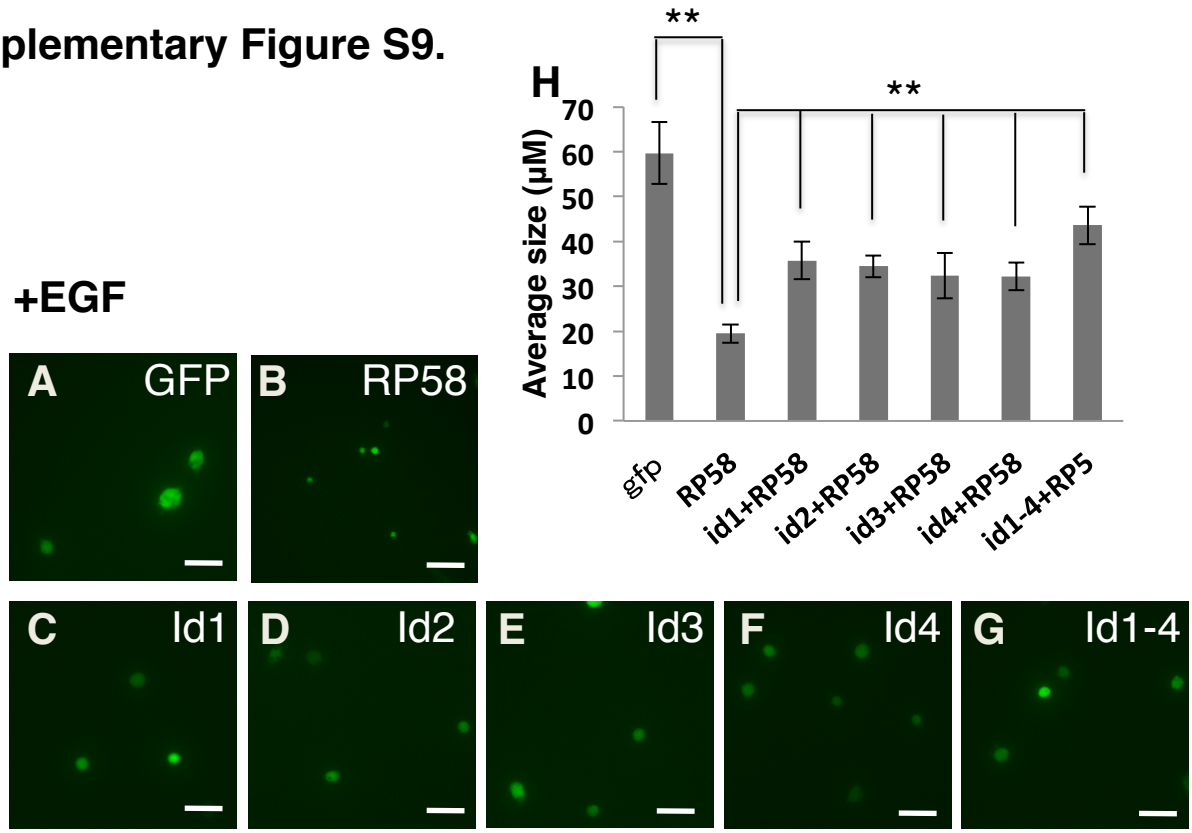

Figure S9. Co-induction of Ids along with Rp58 partially rescued the size of the neurospheres.
(**A-G**) Representative images showing GFP-expressing neurospheres isolated from the E14.5 cortex and cultured for 7 days in the presence of EGF. (**B**) shows Rp58-induced spheres, and (**C-G**) show Id- and Rp58-induced spheres. Three experiments were performed for each of the four embryos. (**H**) Quantification of the average of the diameter under the condition in (**A-G**). (**$P < 0.01$; *t*-test). Error bars indicate the SD. Scale bars: 100 μm.

Supplementary Figure S10.

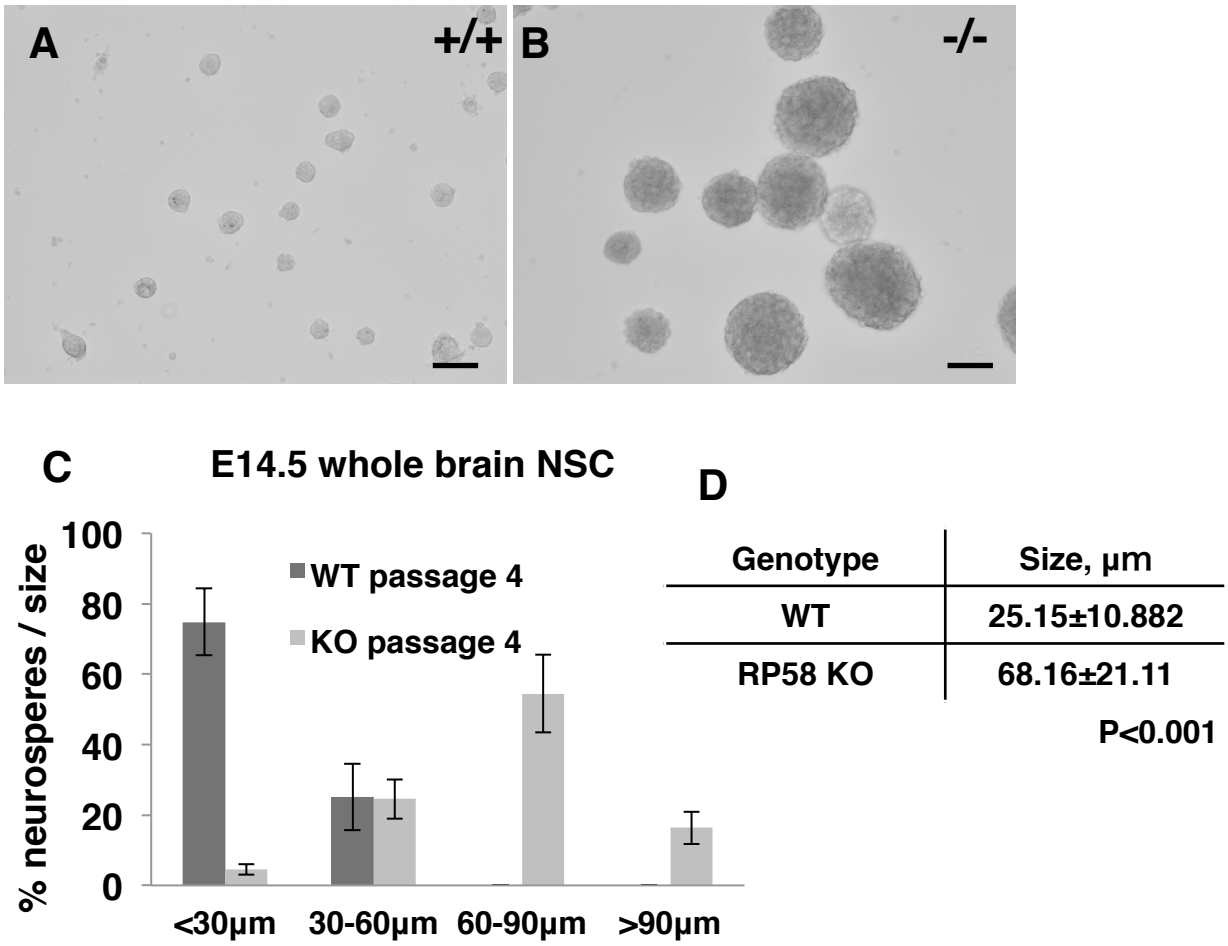

Figure S10. Self-renewal potential of NSCs from the Rp58 KO cortex.
(**A, B**) Neurospheres from E14.5 at passage 4. Representative images showing neurospheres from WT and KO E14.5 cortex cultures. (**C**) Size distribution of E14.5 neurospheres after four passages. Scale bars: 50 µm (*n*=3). Rp58 KO spheres were much larger than wild-type spheres as shown by a shift to the right in the size distribution plot. (**D**) The average diameter of >200 neurospheres per genotype. The Rp58 KO neurospheres were also roughly 2.7-fold larger in volume (***P* < 0.01; *t*-test), indicating enhanced self-renewal.

Supplementary Figure S11.

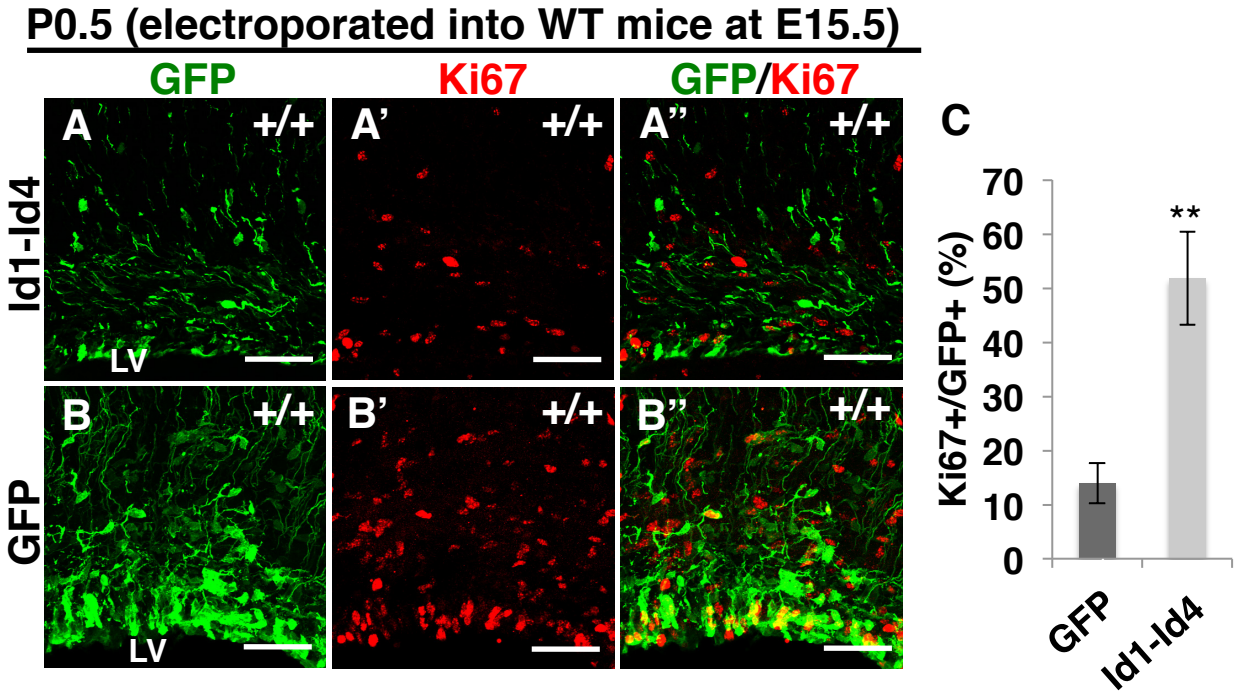

Figure S11. ***Id* overexpression mimicked the *Rp58* KO mouse phenotype of increased proliferating cells.**
(**A, B, A", B"**) Representative images of WT brains electroporated at E15.5 with *GFP* expression vector (**A-A"**) or co-electroporated with *GFP*, *Id1*, *Id2*, *Id3*, and *Id4* expression vectors (**B-B"**) were fixed at P0.5 and stained with anti-GFP (green) (**A, B, A", B"**) and anti-Ki67 (red) (**A', B', A", B"**) at P0.5. (**C**) Quantification of the ratio of Ki67-positive cells to GFP-positive cells in (**A"**) and (**B"**). Scale bars: 50 μm (**A-B"**). *t*-test: (**) $P < 0.01$. Error bars represent mean ± SD, $n = 4$. LV; lateral ventricle.

Supplementary Figure S12.

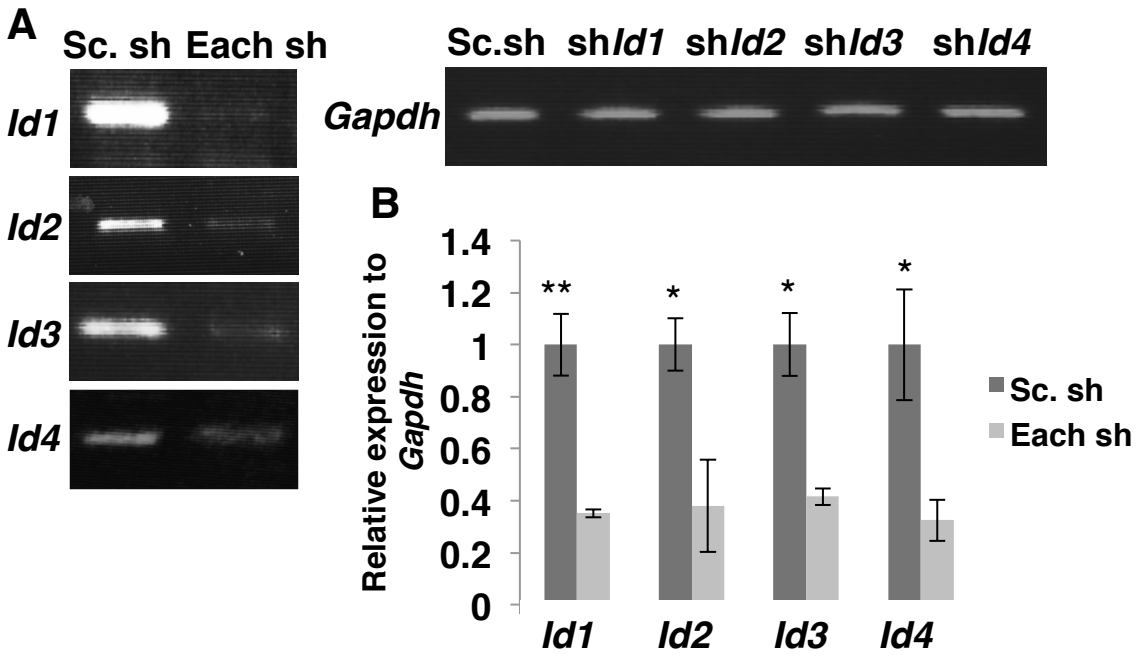

Figure S12. **Downregulatory effect of sh*Id* expression in mouse NSC-derived neurospheres.**
(**A**) RT-PCR analysis showed that the dissociated cells from E14.5 WT cerebral cortex transduced with either GFP-IRES-scramble shRNA (Sc. sh) lentivirus or sh*Id1, Id2, Id3* and *Id4*-IRES-GFP (sh*Id1-Id4*) lentivirus produced neurospheres, which were harvested after 4 days. (**B**) Semi-quantification of the presented agarose gel image (**A**) was performed using Fiji software. *t*-test: (*) $P < 0.05$, (**) $P < 0.01$. Error bars indicate mean ± SD, $n = 3$.

Supplementary Figure S13.

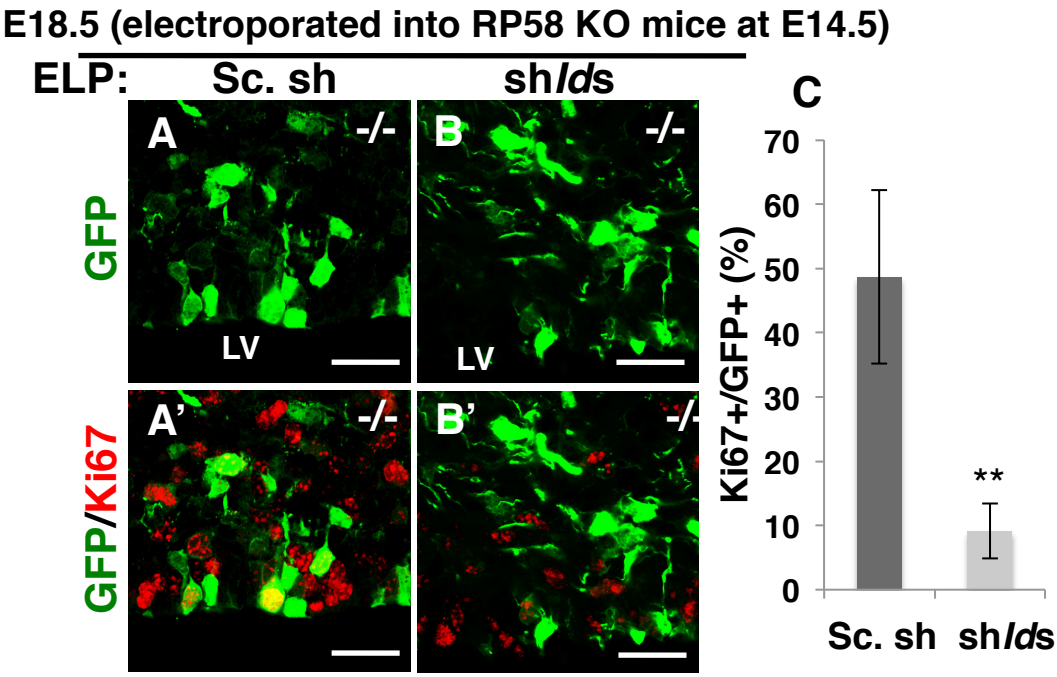

Figure S13. ***Id1-Id4*** **knockdown rescued the increase of proliferating cells in** ***Rp58*** **KO mice.**
(**A-B**') *Rp58* KO cortex electroporated at E14.5 with control scramble shRNA (Sc. sh) expression vector (**A, A**') or co-electroporated with sh*Id1*, sh*Id2*, sh*Id3*, and sh*Id4* expression vectors (**B, B**') was fixed at E18.5 and stained with anti-GFP (green) and anti-Ki67 (red) antibodies. (**C**) Quantification of the ratio of Ki67-positive cells to GFP-positive cells in (**A'**) and (**B'**). Scale bars: 25 μm (**A-B'**). *t*-test: (**) $P < 0.01$. Error bars indicate mean ± SD, $n = 3$. LV; lateral ventricle.

Supplementary Figure S14.

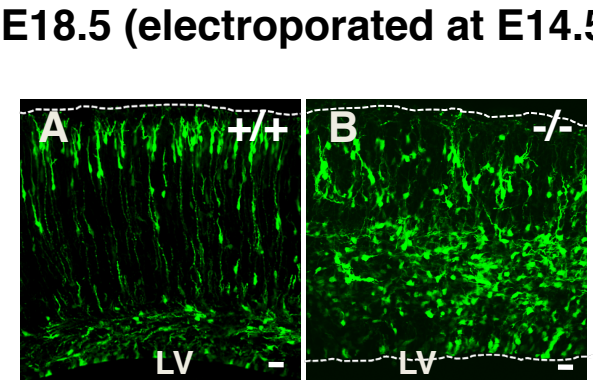

Figure S14. Comparison of the migration pattern in WT and *Rp58* KO cortex. (**A, B**)Representative image of *Rp58* KO cortex electroporated at E14.5 with GFP expression vector was fixed at E18.5 and stained with anti-GFP (green). Scale bars: 25 μm (**A, B**). The dotted lines indicate the edge of the neocortical VZ or cortical plate. LV; lateral ventricle.

Supplementary Figure S15.

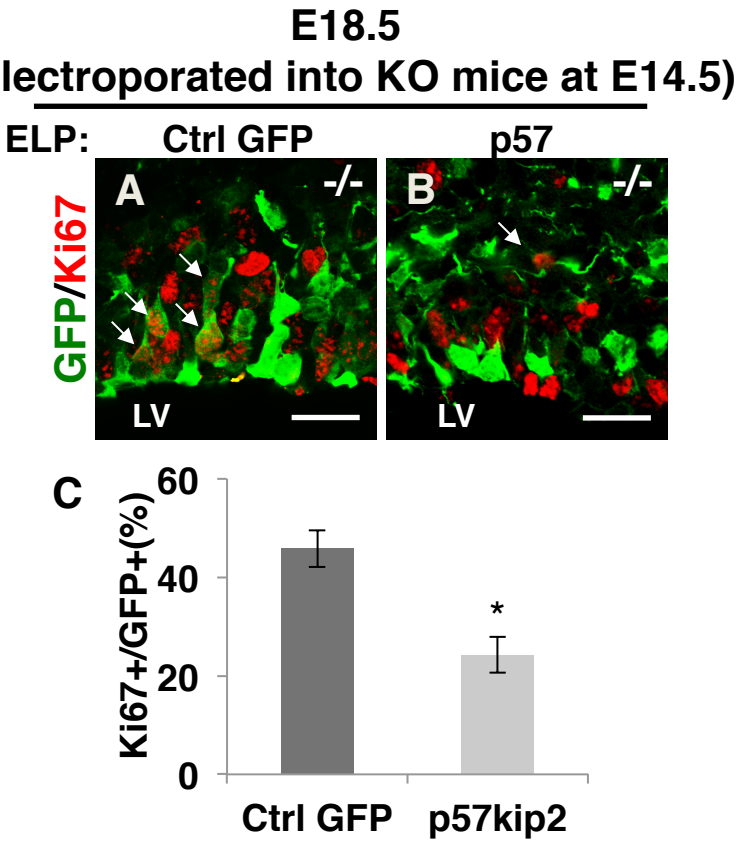

Figure S15. ***p57*** **overexpression rescued the increase of proliferating cells in** ***Rp58*** **KO mice.**
(**A-B**) Representative image of *Rp58* KO cortex electroporated at E14.5 with control *GFP* expression vector (**A**) or co-electroporated with *p57* expression vectors (**B***)* was fixed at E18.5 and stained with anti-GFP (green) and anti-Ki67 (red) antibodies. (**C**) Quantification of the ratio of Ki67-positive cells to GFP-positive cells in (**A**) and (**B***)*. Scale bars: 25 µm (**A, B**). *t*-test: (*) $P < 0.05$. Error bars indicate mean ± SD, $n = 3$. The arrows indicate the double-stained cells.

Supplementary Figure S16.

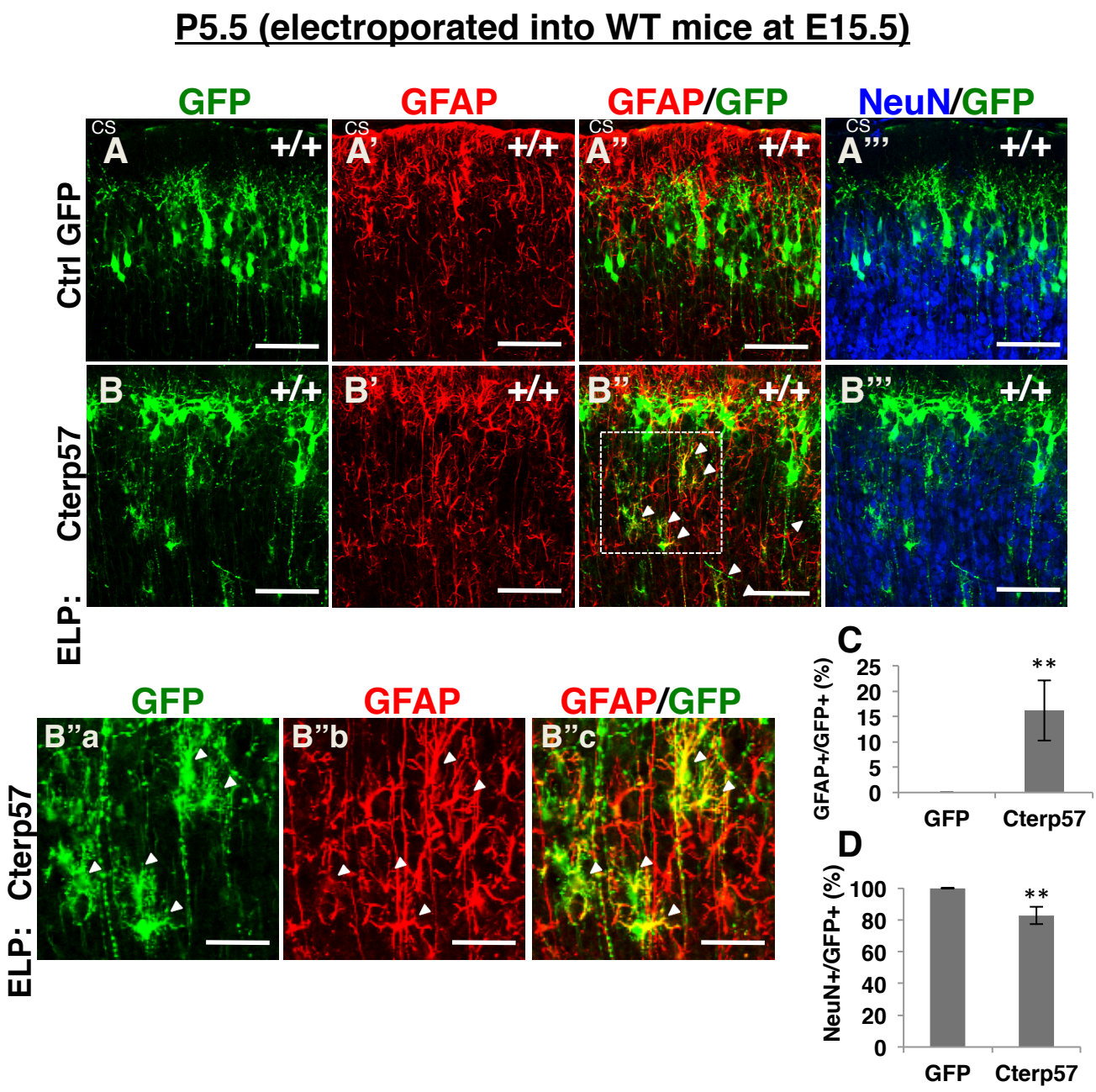

Figure S16. Functional inhibition of p57 protein mimics the Rp58 KO mouse phenotype. (**A-B"c**) Representative fluorescence images of coronal sections through cortices electroporated with control GFP or Cterp57 at E15.5 and analyzed after 9 days. Sections were double-labeled for GFP, GFAP and NeuN. (**B"a-B"c)** Magnification of the dotted square in (**B"**). (**C and D**) Percentage of EGFP or NeuN-positive cells within the cortical mantle. GFAP and GFP double-positive cells indicated by arrowheads (**B", B"a-B"c**) (*n*=3). $^{*}P<0.05$, $^{**}P<0.01$. Error bars indicate ± SD. Scale bars: 100 µm (**A-B'"**), 50 m (**B"a-B"c**). CS; cortical surface.

Supplementary Figure S17.

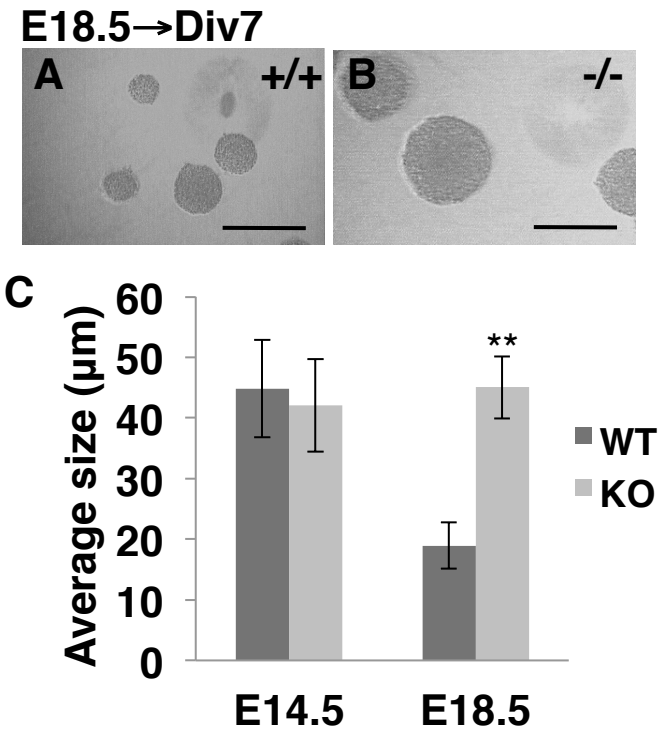

Figure S17. **Progenitors from the E18.5 cortex maintain proliferative competency to the same extent as those from E14.5 in *Rp58* KO mice.**
(**A, B**) Representative images showing neurospheres harvested from E18.5 cortex of WT (**A**) or *Rp58* KO mice (**B**). The neurospheres were harvested from E14.5 or E18.5 after 7 days. Scale bars: 50 μm. (**C**) Quantitative analysis of neurosphere diameter. (**$P < 0.01$; *t*-test). Error bars indicate SD (n=20).

Supplementary Figure S18.

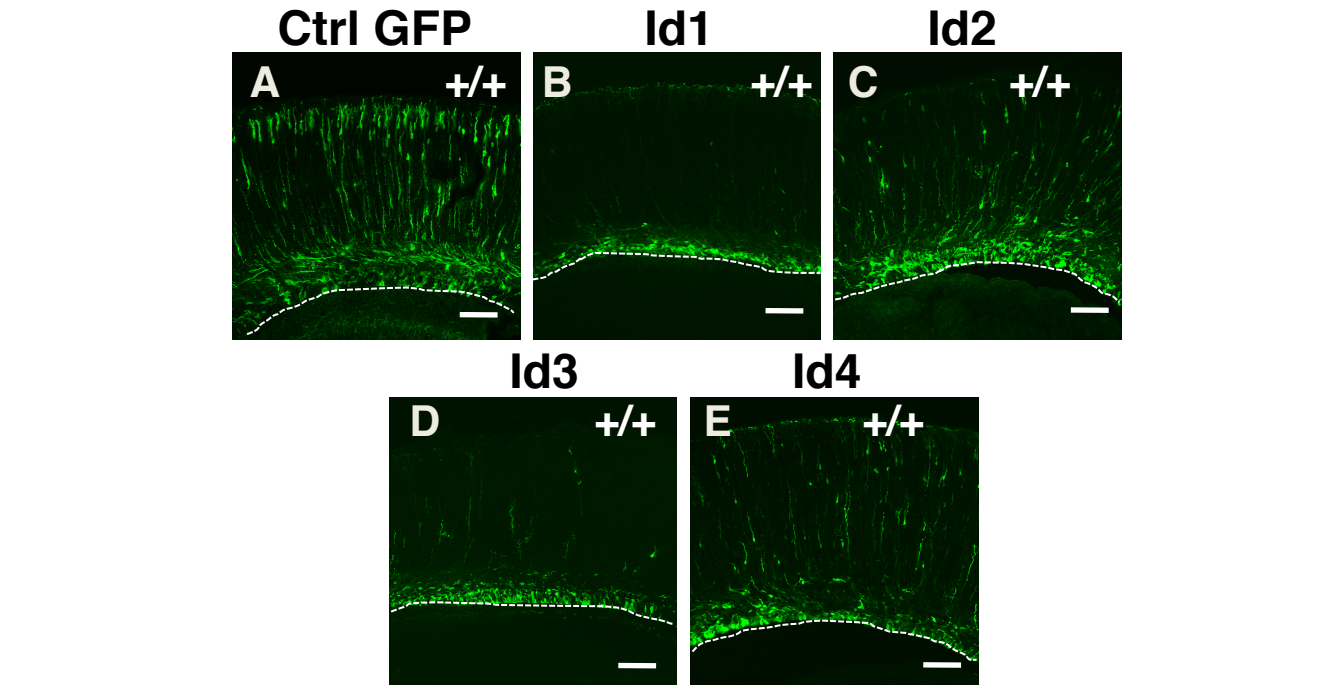

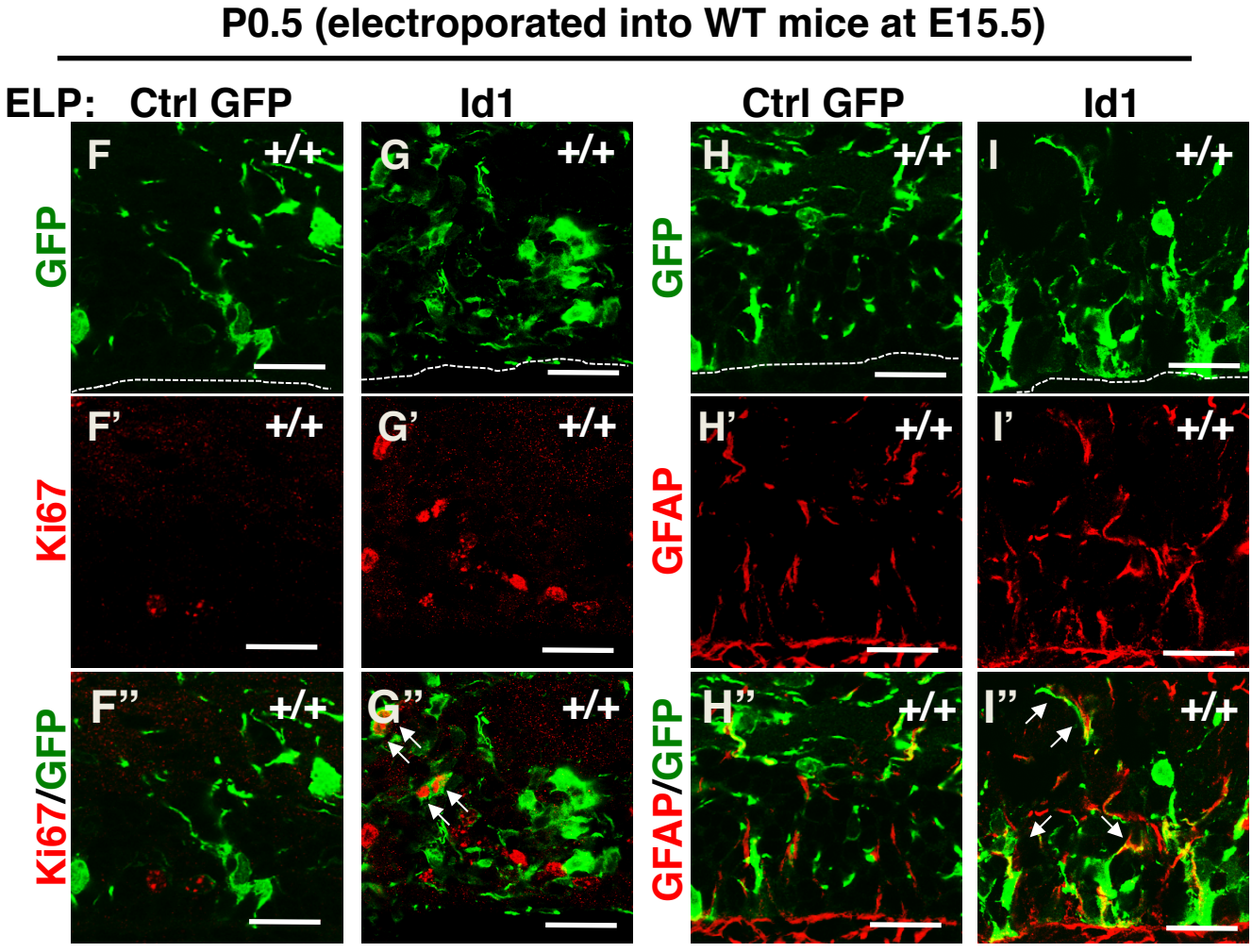

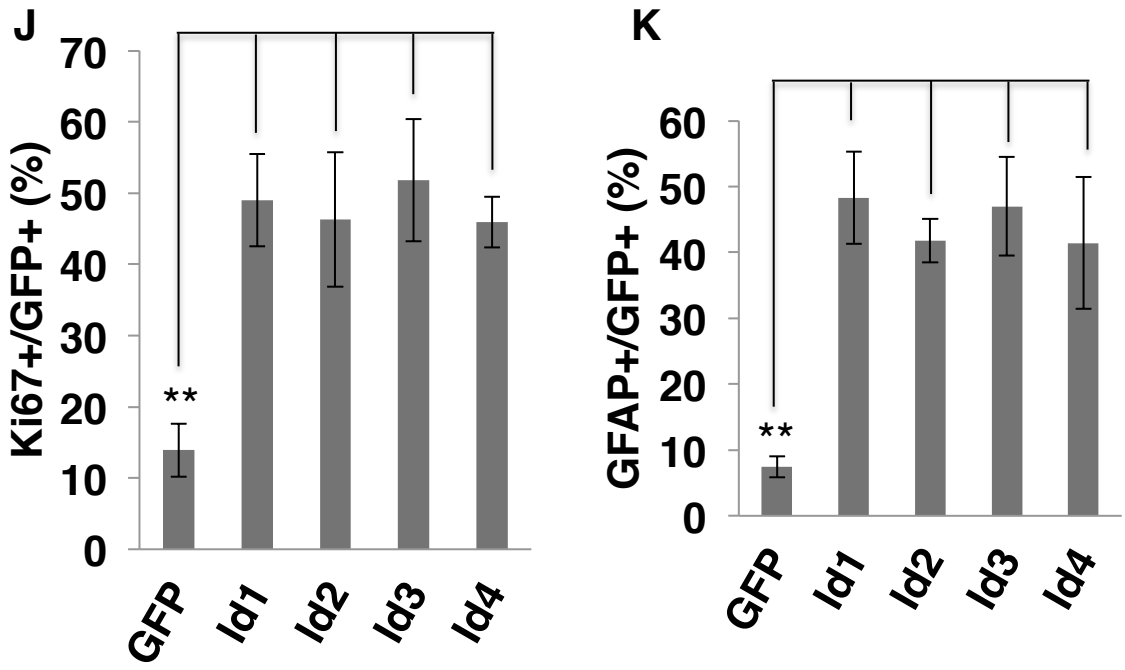

Figure S18. Expression of each Id *in vivo* impacts on the progenitor/astrocyte compartments.

(**A-K**) E15.5 WT cortices were electroporated with control GFP or with each Id, and GFP overexpression was analyzed 4 days later. (**A-E**) Representative images showing labeling of the GFP signal in coronal cortical sections (n=3). (**F-I"**) Representative magnified images of the VZ/SVZ regions from A. (**J,K**) Quantification of Ki67$^+$/GFP$^+$ cells or GFAP$^+$/GFP$^+$ cells within the VZ/SVZ. Scale bars: 100 µm (**A-E**), 25 µm (**F-I"**). (**$P < 0.01$; t-test). Data represent the mean ± SD (n=3). The dotted lines indicate the edge of the neocortical VZ or cortical plate.

Supplementary Figure S19.

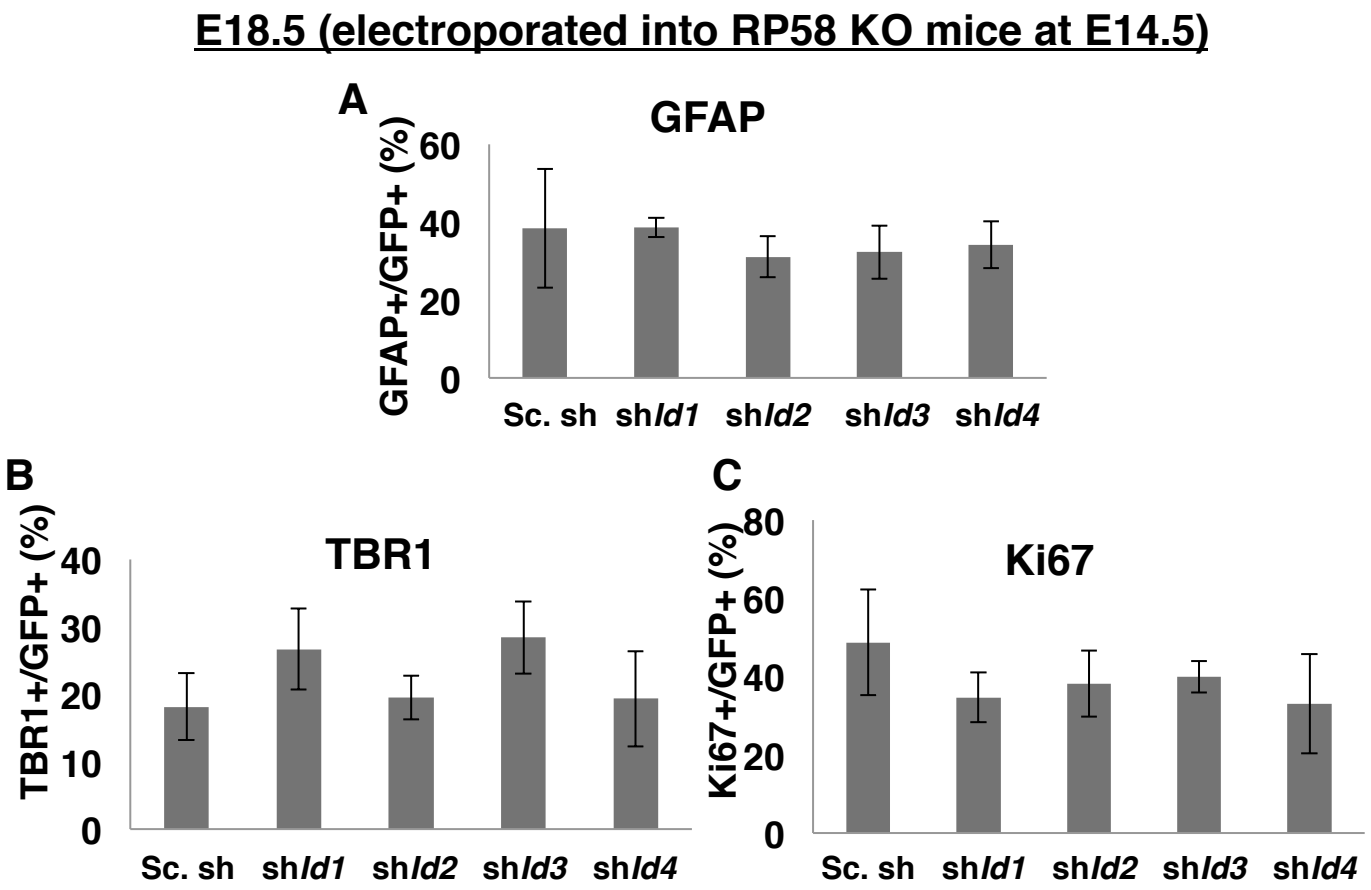

Figure S19. **Knockdown of each *Id* gene could not rescue the *Rp58* KO phenotype.** (**A-C**) *Rp58* KO cortex electroporated at E14.5 with control scramble (Sc) shRNA, sh*Id1*, sh*Id2*, sh*Id3*, or sh*Id4* was fixed at E18.5 and stained with anti-GFP and anti-GFAP, anti-Tbr1 or anti-Ki67. Quantification of the ratio of GFAP-positive cells to GFP-positive cells (**A**), the ratio of Tbr1-positive cells to GFP-positive cells in (**B**) and the ratio of Ki67-positive cells to GFP-positive cells in (**C**). Error bars indicate SD, $n = 3$.

Supplementary Figure S20.

Table S4. Colony formation of *Rp58* KO mouse derived progenitors.

Group	No. of Colonies per field (×40)
	Mean ± SD
Hela cells (positive control)	15.3 ± 2.8
WT	0**
Rp58 KO	0**

**P < 0.01, compared to the positive control (Hela cells).

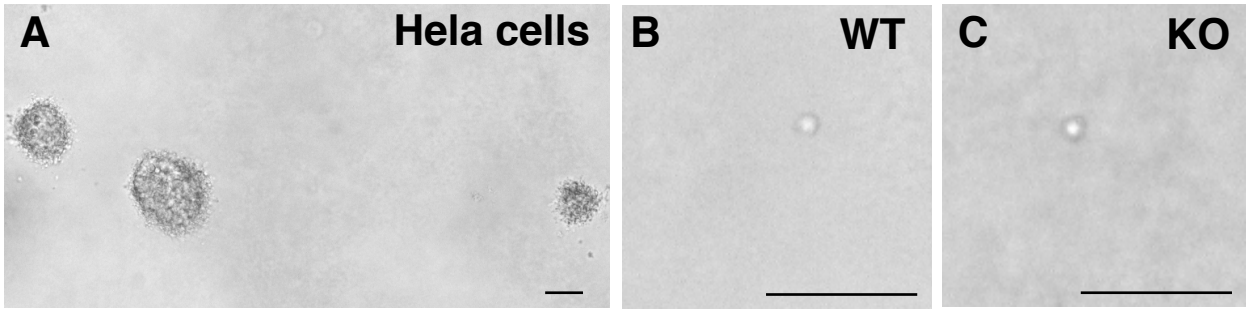

Figure S20. Progenitor cells from the Rp58 KO cortex do not display anchorage-independent growth.
(**A-C**) The results of a colony formation assay characterizing the Rp58 KO progenitor cells. Representative DIC images of colony-forming HeLa cells (**A**) and non-colony forming WT and Rp58 KO cells **(B, C**). Scale bars: 50 µm.